ChemComm

COMMUNICATION

View Article Online
View Journal | View Issue

Cite this: *Chem. Commun.*, 2015, **51**, 2714

Received 6th December 2014,
Accepted 3rd January 2015

DOI: 10.1039/c4cc09774b

www.rsc.org/chemcomm

Highly selective adsorption of ethylene over ethane in a MOF featuring the combination of open metal site and π-complexation†

Yiming Zhang,[a] Baiyan Li,*[ab] Rajamani Krishna,[c] Zili Wu,[d] Dingxuan Ma,[b] Zhan Shi,[b] Tony Pham,[a] Katherine Forrest,[a] Brian Space[a] and Shengqian Ma*[a]

The introduction of the combination of open metal site (OMS) and π-complexation into MOF has led to very high ethylene–ethane adsorption selectivity at 318 K, as illustrated in the context of MIL-101–Cr–SO_3Ag. The interactions with ethylene from both OMS and π-complexation in MIL-101–Cr–SO_3Ag have been investigated by *in situ* IR spectroscopic studies and computational calculations, which suggest that π-complexation contributes dominantly to the high ethylene–ethane adsorption selectivity.

The separation of ethylene–ethane mixtures represents an important industrial process, and is also considered as one of the most challenging chemical separations in the large scale because of the similar molecular sizes and volatilities between ethylene and ethane.[1] The current technology in industry is dictated by cryogenic distillation, which is cost and energy intensive due to the requirement of high pressure and low temperature.[2] Among several alternative approaches[3,4] under development for energy-efficient ethylene–ethane separation at higher temperatures (at or above room temperature), adsorptive separation using porous solid materials has attracted particular attention.[5]

Due to their high surface areas, tunable pore sizes, and functionalizable pore surfaces as well as the amenability of design and modular nature, metal–organic frameworks (MOFs)[6] have been recently explored as a new type of porous solid materials for hydrocarbon separation,[7] including the separation of ethylene–ethane mixtures.[8] Extensive efforts have been devoted to the creation of open metal sites (OMSs) in MOFs to enhance the selectivity of ethylene over ethane, due to the stronger interactions of ethylene with OMSs compared with ethane.[8a] Recently, we demonstrated that a Ag(I) ion functionalized porous aromatic framework (PAF) exhibited exceptional ethylene–ethane adsorption selectivity as a result of the formation of π-complexation between ethylene molecules and Ag(I) ions.[9] We speculate that if such a kind of π-complexation can be coupled with OMSs into MOFs, the adsorption selectivity of ethylene over ethane can be further enhanced in MOFs because of the strong interactions with ethylene from both π-complexation and OMSs. In this contribution, we report the introduction of the combination of OMSs and π-complexation into MOF for the first time, as exemplified in the context of MIL-101–Cr–SO_3Ag, which demonstrates exceptional ethylene–ethane adsorption selectivity at 318 K, surpassing benchmark porous solid materials of zeolites, MOFs and PAFs. The interactions with ethylene from both OMSs and π-complexation have been investigated using *in situ* IR spectroscopic studies and computational calculations.

MIL-101–Cr–SO_3Ag was afforded *via* Ag(I) ion exchange of the sulphonic acid functionalized MIL-101–Cr (MIL-101–Cr–SO_3H), which was prepared using the method reported in the literature[10] (Scheme 1). The powder X-ray diffraction studies show that the patterns of MIL-101–Cr–SO_3Ag are consistent with those of MIL-101–Cr–SO_3H (Fig. S1, ESI†), indicating the maintenance of structural integrity during the Ag(I) exchange process. N_2 gas sorption isotherms collected at 77 K (Fig. S2, ESI†) reveal Brunauer–Emmett–Teller (BET) surface areas of 1570 $m^2\ g^{-1}$ and 1374 $m^2\ g^{-1}$ for MIL-101–Cr–SO_3H and MIL-101–Cr–SO_3Ag, respectively. The decreasing surface area should be presumably due to the introduction of Ag(I) ions. The presence of Ag(I) in MIL-101–Cr–SO_3Ag was confirmed using X-ray photoelectron spectroscopy (XPS) analysis, which shows the silver signals at a binding energy of 368.8 eV and 374.8 eV (Fig. S3, ESI†) corresponding to the peaks of $Ag3d_{5/2}$ and $Ag3d_{3/2}$, respectively. Inductively coupled plasma mass spectrometry (ICP-MS) suggests that ~51% SO_3H were exchanged into SO_3Ag.

[a] *Department of Chemistry, University of South Florida, 4202 E. Fowler Avenue, Tampa, FL 33620, USA. E-mail: sqma@usf.edu, libaiyan@gmail.com; Fax: +1-813-974-3203; Tel: +1-813-974-5217*

[b] *State Key Laboratory of Inorganic Synthesis and Preparative Chemistry, College of Chemistry, Jilin University, Changchun 130012, People's Republic of China*

[c] *Van't Hoff Institute for Molecular Sciences, University of Amsterdam, Science Park 904, 1098 XH Amsterdam, Netherlands*

[d] *Center for Nanophase Materials Science and Chemical Science Division, Oak Ridge National Laboratory, TN 37831, USA*

† Electronic supplementary information (ESI) available: Detailed methods for catalyst preparation, measurements, analysis and catalytic process. See DOI: 10.1039/c4cc09774b

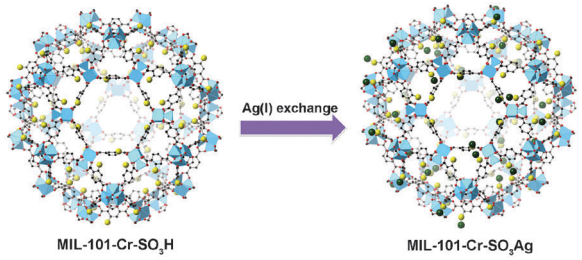

Scheme 1 Schematic illustration of Ag(I) exchange in MIL-101–Cr–SO_3H to afford MIL-101–Cr–SO_3Ag.

The low-pressure ethylene–ethane sorption isotherms were collected at 296 K and 318 K. Compared with the pristine MIL-101–Cr–SO_3H, the introduction of Ag(I) ion into MIL-101–Cr–SO_3H results in a significant enhancement of ethylene adsorption capacity despite the decrease in surface area. Under 1 atm pressure, the ethylene uptake amounts increase from 42 cm^3 g^{-1} at 296 K and 37 cm^3 g^{-1} at 318 K for MIL-101–Cr–SO_3H to 73 cm^3 g^{-1} at 296 K and 63 cm^3 g^{-1} at 318 K for MIL-101–Cr–SO_3Ag (Fig. 1). Interestingly, in contrast to the ethylene adsorption, the uptake amounts of ethane at 296 K and 318 K for two samples are comparable (Fig. S4 and S5, ESI†), suggesting that the introduction of Ag(I) ions would not increase the ethane uptake capacity.

Ethylene–ethane adsorption selectivities were calculated using ideal adsorbed solution theory (IAST)[11] for MIL-101–Cr–SO_3H and MIL-101–Cr–SO_3Ag (Fig. 2). For an equimolar mixture of ethylene and ethane at 318 K, the adsorption selectivity (S_{ads}) obtained for MIL-101–Cr–SO_3Ag is 9.7 at 100 kPa, far exceeding that calculated for MIL-101–Cr–SO_3H (S_{ads} = 1.2). This result suggests the predominant contribution from Ag(I) ion in comparison with the OMS of Cr(III) to the enhancement of ethylene–ethane adsorption selectivity. The ethylene–ethane adsorption selectivity of MIL-101–Cr–SO_3Ag at 318 K and 100 kPa is also significantly higher than those of the zeolite NaX,[8b] the MOFs[8b] CoMOF-74 [also known as (a.k.a.) Co_2(dobdc)], MgMOF-74 [a.k.a. Mg_2(dobdc)], CuBTC (a.k.a. HKUST-1) (Fig. 2), exhibiting ethylene–ethane selectivities of 6.8, 5.7, 4.7, and 3.8, respectively. It slightly surpasses the best

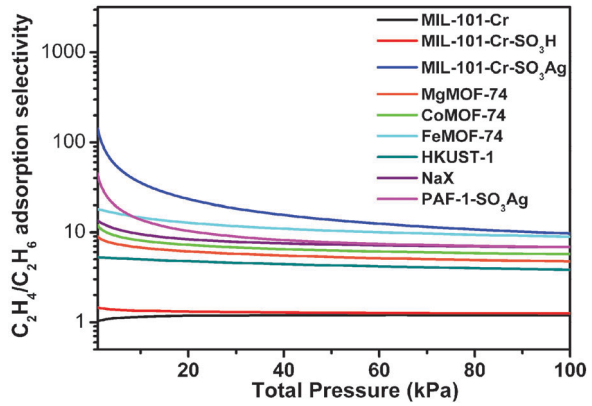

Fig. 2 Comparison of the IAST calculations for C_2H_4–C_2H_6 adsorption selectivities for MIL-101–Cr–SO_3Ag with MIL-101–Cr–SO_3H and other porous materials[10] at 318 K.

performance MOF of FeMOF-74 (a.k.a. Fe_2(dobdc)) (S_{ads} = 8.9) and PAF of PAF-1–SO_3Ag[9] (S_{ads} = 6.9). It is worth noting that the higher ethylene–ethane adsorption selectivities of MIL-101–Cr–SO_3Ag compared to PAF-1–SO_3Ag indicate the possible cooperative contribution from the OMS of Cr(III) to further boosting the ethylene–ethane adsorption selectivities for MIL-101–Cr–SO_3Ag.

To provide a better understanding of the exceptional ethylene adsorption properties of MIL-101–Cr–SO_3Ag, the isosteric heats of adsorption (Q_{st}) were calculated using the Clausius–Clapeyron equation by differentiation of the dual Langmuir–Freundlich fits of the isotherms at two different temperatures,[7c,8b] 296 K and 318 K with T-dependent parameters. As shown in Fig. 3, close to zero loading, the Q_{st} for ethylene in MIL-101–Cr–SO_3Ag is 63 kJ mol^{-1}, remarkably higher than that of MIL-101–Cr–SO_3H (10 kJ mol^{-1}). These results highlight the role of introducing Ag(I) ions in further boosting the interactions with ethylene molecules that stem from the formation of the π-complexation bonding between the d orbital of Ag(I) and the π* orbital of carbon–carbon double bonds in ethylene.[12] In contrast to the high Q_{st} for ethylene, MIL-101–Cr–SO_3Ag shows a significantly lower Q_{st} for ethane with a value of 16 kJ mol^{-1} (Fig. S6, ESI†);

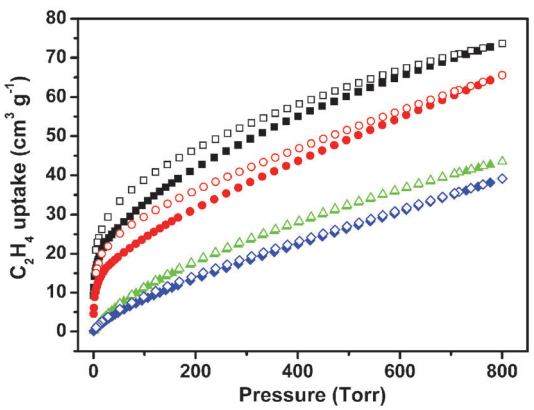

Fig. 1 C_2H_4 sorption isotherms of MIL-101–Cr–SO_3Ag (black: 296 K; red: 318 K) and MIL-101–Cr–SO_3H (green: 296 K; blue 318 K). Filled: adsorption; unfilled: desorption.

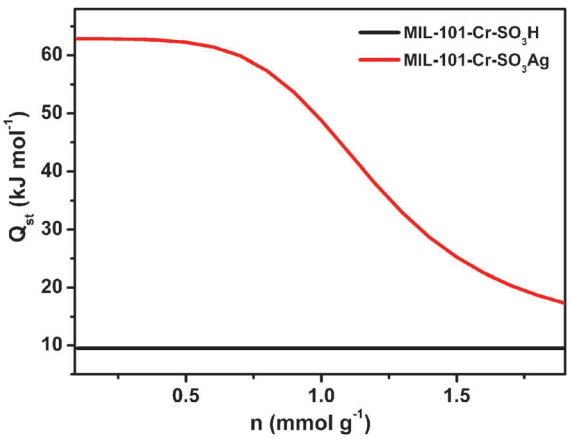

Fig. 3 The isosteric heats of adsorption, Q_{st} of C_2H_4 for MIL-101–Cr–SO_3H, and MIL-101–Cr–SO_3Ag.

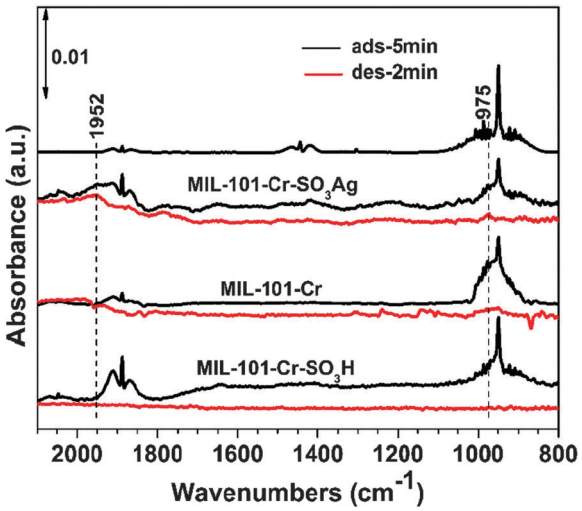

Fig. 4 IR spectra from ethylene adsorption and desorption on MIL-101–Cr, MIL-101–Cr–SO_3H and MIL-101–Cr–SO_3Ag at room temperature. IR spectrum from gas phase ethylene is also shown for reference.

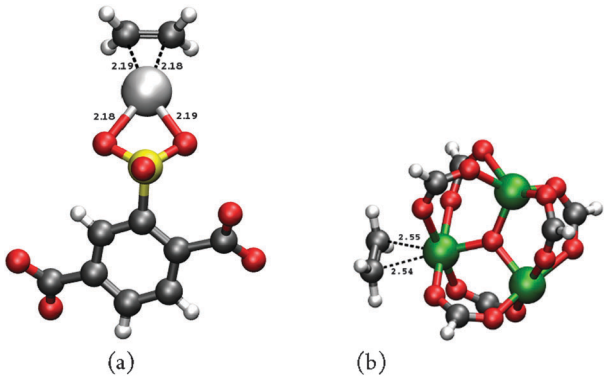

Fig. 5 The optimized position of an ethylene molecule within (a) $(C_6H_3(CO_2)_2)SO_3Ag$ and (b) $[Cr_3O(O_2CH)_6]^+$ clusters.

thus validating that MIL-101–Cr–SO_3Ag featuring the combination of OMS and π-complexation can selectively adsorb ethylene over ethane thereby resulting in high ethylene–ethane adsorption selectivities particularly at a relatively high temperature of 318 K.

In situ IR measurements of ethylene adsorption at room temperature gave further insight into the nature of interactions between ethylene molecules and the Ag(I) ions in MIL-101–Cr–SO_3Ag. As shown in Fig. 4, the appearance of IR features at 975 cm^{-1} corresponds to the ethylene adsorption on the surface of porous materials. MIL-101–Cr–SO_3Ag exhibits a stronger ethylene interaction than that of MIL-101–Cr and MIL-101–Cr–SO_3H, which is evidenced by the complete disappearance of ethylene IR features at 975 cm^{-1} for the two compared samples after room temperature desorption in helium purge gas. The extra IR features at 1952 cm^{-1} (combination mode of $-CH_2$ wagging), not observed on the MIL-101–Cr and MIL-101–Cr–SO_3H, further confirm stronger ethylene interactions on MIL-101–Cr–SO_3Ag. The blue-shift of the $-CH_2$ wagging mode can be attributed to the combinative d–π and d–π* interaction between Ag and ethylene,[13–16] as a result of the formation of π-complexation between the ethylene and Ag(I) ions in MIL-101–Cr–SO_3Ag.

To further understand the interactions of ethylene–Ag(I) ion and ethylene–Cr(III) OMS, we used electronic structure calculations to estimate the bond length between ethylene and Ag(I) as well as the bond length between ethylene and Cr(III). A $(C_6H_3(CO_2)_2)SO_3Ag$ cluster was considered for this calculation since it is expected that MIL-101–Cr–SO_3Ag contains this moiety. Starting with the sulfonyl terephthalate unit, a silver ion was placed in proximity to the oxygen atoms of the sulfonate group. The Ag(I) ion was optimized to an energetically favorable position within the cluster. Afterwards, an optimized ethylene molecule was placed in proximity to the Ag(I) ion in the $(C_6H_3(CO_2)_2)SO_3Ag$ cluster. The optimization of the C_2H_4–Ag(I) interaction was executed using the DFT method. It was observed that the distances between the Ag(I) ion and the carbon atoms of the C_2H_4 molecule were found to be 2.18 and 2.19 Å (Fig. 5a). A similar calculation was performed between the ethylene molecule and the Cr(III) OMSs, and the optimized C_2H_4–Cr(III) distances were observed to be 2.54 and 2.55 Å (Fig. 5b). These results suggest that the interactions between ethylene and Ag(I) are much stronger than those between Cr(III) OMSs and they should contribute dominantly to the high adsorption selectivity of MIL-101–Cr–SO_3Ag for ethylene–ethane.

Given the reasonable accuracy of simulated breakthrough characteristics as validated by recent investigations,[7c,8a,b] we carried out breakthrough simulations for C_2H_4–C_2H_6 mixtures in a fixed bed to demonstrate the feasibility of producing 99.95% + pure C_2H_4 in a Pressure Swing Adsorption (PSA) operation. The simulated breakthrough curves of Fig. S9 (ESI†) show transient breakthrough of an equimolar C_2H_4–C_2H_6 mixture in an adsorber bed packed with MIL-101–Cr–SO_3Ag. During the adsorption cycle, C_2H_6 at purities >99% can be recovered for a certain duration of the adsorption cycle as indicated by the arrow in Fig. S10 (ESI†). In addition, ethylene of 99.95% + purity, required as feedstock to the polymerization reactor, can also be recovered during the time interval indicated by the arrow in Fig. S11 (ESI†) in the desorption cycle.

In summary, we have demonstrated the introduction of open metal site (OMS) and π-complexation into MOF, affording MIL-101–Cr–SO_3Ag as an efficient adsorbent for separation of ethylene–ethane. MIL-101–Cr–SO_3Ag exhibits significantly higher ethylene–ethane adsorption selectivity at 318 K than benchmark zeolites, MOFs and PAFs reported in the literatures. The high ethylene–ethane adsorption selectivity of MIL-101–Cr–SO_3Ag are mainly attributed to the π-complexation between Ag(I) ions and the double bond of ethylene molecules, which is reflected in the high isosteric heats of adsorption of C_2H_4 and evidenced using *in situ* IR spectroscopy studies and computational calculations. In addition, the possible cooperative contribution from the OMS of Cr(III) to further enhancing the ethylene–ethane adsorption selectivities have been proved by the higher ethylene–ethane adsorption selectivities of MIL-101–Cr–SO_3Ag compared to PAF-1–SO_3Ag. The feasibility of MIL-101–Cr–SO_3Ag for producing 99.95% + pure C_2H_4 in a PSA operation has also been demonstrated by breakthrough simulations. Our strategy of introducing dual functional sites into

MOF to afford high ethylene–ethane adsorption selectivities particularly above room temperature paves a new way for developing MOFs for energy-saving ethylene–ethane and other olefin/paraffin separations.

The authors acknowledge the University of South Florida and the National Science Foundation (DMR-1352065) for financial support of this work. A portion of this research including the *in situ* IR work was conducted at the Center for Nanophase Materials Sciences, which is a DOE Office of Science User Facility. B.S. acknowledges the National Science Foundation (Award No. CHE-1152362), the computational resources that were made available by a XSEDE Grant (No. TG-DMR090028), and the use of the services provided by Research Computing at the University of South Florida.

Notes and references

1 R. B. Eldridge, *Ind. Eng. Chem. Res.*, 1993, **32**, 2208.
2 S. U. Rege, J. Padin and R. T. Yang, *AIChE J.*, 1998, **44**, 799.
3 H. Bux, C. Chmelik, R. Krishna and J. Caro, *J. Membr. Sci.*, 2011, **369**, 284.
4 D. J. Safarik and R. B. Eldridge, *Ind. Eng. Chem. Res.*, 1998, **37**, 2571.
5 (*a*) R. T. Yang, *Adsorbents fundamentals and applications*, John Wiley & Sons, Inc., New Jersey, 2003; (*b*) R. Krishna, *Microporous Mesoporous Mater.*, 2014, **185**, 30; (*c*) P. Li, Y. He, H. D. Arman, R. Krishna, H. Wang, L. Weng and B. Chen, *Chem. Commun.*, 2014, **50**, 13081; (*d*) L. Huang and D. Cao, *J. Mater. Chem. A*, 2013, **1**, 9433; (*e*) M. H. Weston, Y. J. Colón, Y.-S. Bae, S. J. Garibay, R. Q. Snurr, O. K. Farha, J. T. Hupp and S. T. Nguyen, *J. Mater. Chem. A*, 2014, **2**, 299; (*f*) S. Aguado, G. Bergeret, C. Daniel and D. Farrusseng, *J. Am. Chem. Soc.*, 2012, **134**, 14635; (*g*) H. Ma, H. Ren, S. Meng, F. Sun and G. Zhu, *Sci. Rep.*, 2013, **3**, 2611; (*h*) B. Li, Y. Zhang, D. Ma, Z. Shi and S. Ma, *Nat. Commun.*, 2014, **5**, 5537.
6 (*a*) H.-C. Zhou, J. R. Long and O. M. Yaghi, *Chem. Rev.*, 2012, **112**, 673; (*b*) H.-C. Zhou and S. Kitagawa, *Chem. Soc. Rev.*, 2014, **43**, 5415; (*c*) W.-Y. Gao, M. Chrzanowski and S. Ma, *Chem. Soc. Rev.*, 2014, **43**, 5841; (*d*) W.-Y. Gao and S. Ma, *Comments Inorg. Chem.*, 2014, **34**, 125.
7 (*a*) H. Wu, Q. Gong, D. H. Olson and J. Li, *Chem. Rev.*, 2012, **112**, 836; (*b*) Z. R. Herm, E. D. Bloch and J. R. Long, *Chem. Mater.*, 2014, **26**, 323; (*c*) Z. Zhang, Z. Z. Yao, S. Xiang and B. Chen, *Energy Environ. Sci.*, 2014, **7**, 2868; (*d*) C. Y. Lee, Y.-S. Bae, N. C. Jeong, O. K. Farha, A. A. Sarjeant, C. L. Stern, P. Nickias, R. Q. Snurr, J. T. Hupp and S. T. Nguyen, *J. Am. Chem. Soc.*, 2011, **133**, 5228; (*e*) Y.-S. Bae, C. Y. Lee, K. C. Kim, O. K. Farha, P. Nickias, J. T. Hupp, S. T. Nguyen and R. Q. Snurr, *Angew. Chem., Int. Ed.*, 2012, **51**, 1857; (*f*) S.-C. Xiang, Z. Zhang, C.-G. Zhao, K. Hong, X. Zhao, D.-R. Ding, M.-H. Xie, C.-D. Wu, M. C. Das, R. Gill, K. Mark Thomas and B. Chen, *Nat. Commun.*, 2011, **2**, 204; (*g*) K. Li, D. H. Olson, J. Seidel, T. J. Emge, H. Gong, H. Zeng and J. Li, *J. Am. Chem. Soc.*, 2009, **131**, 10368; (*h*) M. Maes, L. Alaerts, F. Vermoortele, R. Ameloot, S. Couck, V. Finsy, J. F. M. Denayer and D. E. De Vos, *J. Am. Chem. Soc.*, 2010, **132**, 2284; (*i*) J. W. Yoon, Y.-K. Seo, Y. K. Hwang, J.-S. Chang, H. Leclerc, S. Wuttke, P. Bazin, A. Vimont, M. Daturi, E. Bloch, P. L. Llewellyn, C. Serre, P. Horcajada, J.-M. Grenèche, A. E. Rodrigues and G. Férey, *Angew. Chem., Int. Ed.*, 2010, **49**, 5949; (*j*) H.-R. Fu, Y. Kang and J. Zhang, *Inorg. Chem.*, 2014, **53**, 4209.
8 (*a*) E. D. Bloch, W. L. Queen, R. Krishna, J. M. Zadrozny, C. M. Brown and J. R. Long, *Science*, 2012, **335**, 1606; (*b*) Y. He, R. Krishna and B. Chen, *Energy Environ. Sci.*, 2012, **5**, 9107; (*c*) S. J. Geier, J. A. Mason, E. D. Bloch, W. L. Queen, M. R. Hudson, C. M. Browncd and J. R. Long, *Chem. Sci.*, 2013, **4**, 2054; (*d*) C. Gücüyener, J. van den Bergh, J. Gascon and F. Kapteijn, *J. Am. Chem. Soc.*, 2010, **132**, 17704; (*e*) U. Böhme, B. Barth, C. Paula, A. Kuhnt, W. Schwieger, A. Mundstock, J. Caro and M. Hartmann, *Langmuir*, 2013, **29**, 8592; (*f*) Z. Bao, S. Alnemrat, L. Yu, I. Vasiliev, Q. Ren, X. Lu and S. Deng, *Langmuir*, 2011, **27**, 13554; (*g*) K. Kishida, S. Horike, Y. Watanabe, M. Tahara, Y. Inubushi and S. Kitagawa, *Chem. – Asian J.*, 2014, **9**, 1643; (*h*) S. Yang, A. J. Ramirez-Cuesta, R. Newby, V. Garcia-Sakai, P. Manuel, S. K. Callear, S. I. Campbell, C. C. Tang and M. Schröder, *Nat. Chem.*, 2014, DOI: 10.1038/NCHEM.2114.
9 B. Li, Y. Zhang, R. Krishna, K. Yao, Y. Han, Z. Wu, D. Ma, Z. Shi, T. Pham, B. Space, J. Liu, P. K. Thallapally, J. Liu, M. Chrzanowski and S. Ma, *J. Am. Chem. Soc.*, 2014, **136**, 8654.
10 G. Akiyama, R. Matsuda, H. Sato, M. Takata and S. Kitagawa, *Adv. Mater.*, 2011, **23**, 3294.
11 A. L. Myers and J. M. Prausnitz, *AIChE J.*, 1965, **11**, 121.
12 S. Uchida, R. Kawamoto, H. Tagami, Y. Nakagawa and N. Mizuno, *J. Am. Chem. Soc.*, 2008, **130**, 12370.
13 D. Stacchiola, G. Wu, M. Kaltchev and W. T. Tysoe, *Surf. Sci.*, 2001, **486**, 9.
14 K. Itoh, T. Kiyohara, H. Shinohara, C. Ohe, Y. Kawamura and H. Nakai, *J. Phys. Chem. B*, 2002, **106**, 10714.
15 Y. Huang, *J. Catal.*, 1980, **61**, 461.
16 E. L. Uzunova and H. Mikosch, *ACS Catal.*, 2013, 2759.

Electronic Supplementary Information

Highly Selective Adsorption of Ethylene over Ethane in a MOF Featuring the Combination of Open Metal Site and π-Complexation

Yiming Zhang,[a] Baiyan Li,[a,d,*] Rajamani Krishna,[b] Zili Wu,[c] Dingxuan Ma,[d] Zhan Shi,[d] Tony Pham,[a] Katherine Forrest,[a] Brian Space,[a] and Shengqian Ma[a,*]

[a]Department of Chemistry, University of South Florida, 4202 E. Fowler Avenue, Tampa, FL 33620, USA.

[b]Van't Hoff Institute for Molecular Sciences, University of Amsterdam, Science Park 904, 1098 XH Amsterdam, Netherlands.

[c]Center for Nanophase Materials Science and Chemical Science Division, Oak Ridge National Laboratory, TN 37831, USA.

[d]State Key Laboratory of Inorganic Synthesis and Preparative Chemistry, College of Chemistry, Jilin University, Changchun 130012, People's Republic of China.

E-mail: sqma@usf.edu; libaiyan@gmail.com

Experimental Details

All Starting materials, reagents, and solvents were purchased from commercial sources (Aldrich, Alfa, Fisher and Acros) and used without further purification.

Synthesis of MIL-101-Cr-SO_3H

MIL-101-Cr-SO_3H was synthesized according to the procedures reported the literature.[1]

Synthesis of MIL-101-Cr-SO_3Ag

To the 15 ml CH_3CN/H_2O (1:1) solution, 100 mg MIL-101-Cr-SO_3H and 100 mg $AgBF_4$ were added. The mixture was stirred under room temperature for 12 h, and then the solid was collected by filtration followed by washing with CH_3CN and water. The whole process was performed carefully under dark place. This exchanged process was conducted for three times, and then dried at 110 ºC for further test. ICP: Cr: 11%; Ag: 11.6%.

Characterization Details

PXRD data were collected on a Rigaku D/max 2550 Powder X-ray Diffractometer. N_2, C_2H_4, and C_2H_6 gas sorption isotherms were collected on a Micrometrics ASAP2020 Surface Area Analyzer. Elemental analyses were performed on a Perkin-Elmer 2400 element analyzer. XPS measurements were performed on an ESCALAB 250 X-ray photoelectron spectroscopy, using Mg Kα X-ray as the excitation source.

In situ IR experiments

IR spectra of ethylene adsorption were collected using a Thermo Nicolet Nexus 670 spectrometer in diffuse reflectance mode (DRIFTS). The MIL-101-Cr-SO_3Ag sample, ca. 5 mg, was treated in a DRIFTS cell (HC-900, Pike Technologies) at 423 K in helium (30 mL/min) for 1 hour to removal water and other adsorbates. The sample was then cooled down to room temperature for ethylene adsorption. The adsorption was conducted by flowing 10% ethylene/He (30 mL/min) over the sample for 5 min and then desorption was done in flowing helium. IR spectra were recorded continuously to follow the surface changes during the adsorption and desorption process. All reported IR spectra are difference spectra referenced to

a background spectrum collected at room temperature after pre-treatment but prior to ethylene adsorption.

Fitting of pure component isotherms

The measured experimental isotherm data for C_2H_4, and C_2H_6 on MIL-101-Cr-SO_3Ag were fitted with the dual-Langmuir-Freundlich isotherm model

$$q = q_{A,sat}\frac{b_A p^{\nu_A}}{1+b_A p^{\nu_A}} + q_{B,sat}\frac{b_B p^{\nu_B}}{1+b_B p^{\nu_B}} \qquad (1)$$

For fitting of the corresponding isotherms for C_2H_6 on MIL-101-Cr-SO_3Ag, a simpler 1-site Langmuir-Freundlich model was of adequate accuracy. The fit parameters for C_2H_4, and C_2H_6 are specified in Table S1. Fig. S7 presents a comparison of the experimentally determined component loadings for C_2H_4, and C_2H_6 on MIL-101-Cr-SO_3Ag at 296 K with the isotherm fits using parameters specified in Table 0. The fits are excellent over the entire range of pressures.

The pure component isotherm data for MIL-101-Cr, and MIL-101-Cr-SO_3H could be fitted with single site Langmuir-Freundlich model; the fit parameters are provided in Table S2, and Table S3, respectively.

Calculations of adsorption selectivity

The selectivity of preferential adsorption of C_2H_4 (component 1) over C_2H_6 (component 2) in a mixture containing 1 and 2, can be formally defined as

$$S_{ads} = \frac{q_1/q_2}{p_1/p_2} \qquad (2)$$

In equation (2), q_1 and q_2 are the component loadings of the adsorbed phase in the mixture. The calculations of S_{ads} are based on the use of the Ideal Adsorbed Solution Theory (IAST) of Myers and Prausnitz.[2]

Isosteric heats of adsorption

The isosteric heat of adsorption, Q_{st}, were calculated using the Clausius-Clapeyron equation by differentiation of the dual-Langmuir-Freundlich fits of the isotherms at two different temperatures, 296 K and 318 K with T-dependent parameters.

Simulations of C_2H_4/C_2H_6 breakthroughs in packed beds

In order to demonstrate the feasibility of producing 99.95%+ pure C_2H_4 in a Pressure Swing Adsorption (PSA) we carried out breakthrough simulations for C_2H_4/C_2H_6 mixtures in a fixed bed of length L, packed with MIL-101-Cr-SO_3Ag that has a framework density ρ = 700 kg/m^3; see schematic in Fig. S8. The voidage of the fixed bed was chosen $\varepsilon = 0.75$.

Assuming plug flow of the binary gas mixture through the fixed bed maintained under isothermal conditions at 296 K, the partial pressures in the gas phase at any position and instant of time are obtained by solving the following set of partial differential equations for each of the species i in the gas mixture.[3-9]

$$\frac{1}{RT}\frac{\partial p_i(t,z)}{\partial t} = -\frac{1}{RT}\frac{\partial\left(v(t,z)\,p_i(t,z)\right)}{\partial z} - \frac{(1-\varepsilon)}{\varepsilon}\rho\frac{\partial \bar{q}_i(t,z)}{\partial t}; \quad i = 1,2,...n \qquad (3)$$

In equation (3), t is the time, z is the distance along the adsorber, ρ is the framework density, ε is the bed voidage, v is the interstitial gas velocity, and $\bar{q}_i(t,z)$ is the *spatially averaged* molar loading within the crystallites of radius r_c, monitored at position z, and at time t. If the values of intra-crystalline diffusivities are large enough to ensure that

intra-crystalline gradients are absent and the entire crystallite particle can be considered to be in thermodynamic equilibrium with the surrounding bulk gas phase at that time *t*, and position *z* of the adsorber

$$\bar{q}_i(t,z) = q_i(t,z) \qquad (4)$$

The molar loadings q_i are calculated on the basis of adsorption equilibrium with the bulk gas phase partial pressures p_i at that position *z* and time *t*. The adsorption equilibrium can be calculated on the basis of the IAST. After discretization of the fixed bed into 100-200 slices, Equations (3) and Equation (4) need to be solved simultaneously using robust numerical procedures that are described in detail in the published literature.[10] The breakthrough simulation methodology has been rigorously tested and validated using a variety of experimental data on breakthroughs.[10]

The breakthrough characteristics for any component is essentially dictated by the characteristic contact time $\frac{L}{v} = \frac{L\varepsilon}{u}$ between the crystallites and the surrounding fluid phase. It is common to use the dimensionless time, $\tau = \frac{tu}{L\varepsilon}$, obtained by dividing the actual time, *t*, by the characteristic time, $\frac{L\varepsilon}{u}$ when plotting simulated breakthrough curves as has been done in Fig. S9.[10,11]

Let us first consider the adsorption phase of the PSA operations. Fig. S9 shows transient breakthrough of an equimolar C_2H_4/C_2H_6 mixture in an adsorber bed packed with MIL-101-Cr-SO_3Ag. The inlet gas is maintained at partial pressures $p_1 = p_2 = 50$ kPa. The more poorly adsorbed saturated alkane breaks through earlier and can be recovered in nearly pure form. From the gas phase concentrations at the exit of the adsorber, we can determine the % C_2H_6; this information is presented in Fig. S10. During the adsorption cycle, C_2H_6 at

purities > 99% can be reovered for a certain duration of the adsorption cycle indicated by the arrow in Fig. S10.

Once the entire bed is in equilibrium with the partial pressures $p_1 = p_2 = 50$ kPa, the desorption, "blowdown" cycle is initiated, by applying a vacuum or purging with inert gas. Fig. S11 shows $\%C_2H_4$ in the outlet gas of an adsorber bed packed with MIL-101-Cr-SO_3Ag in the desorption cycle. For production of ethylene as feedstock for polymerization purposes, the required purity level is 99.95%+ can be recovered during the time interval indicated by the arrow in Fig. S11.

Notation

b_A	dual-Langmuir-Freundlich constant for species *i* at adsorption site A, $Pa^{-\nu_i}$
b_B	dual-Langmuir-Freundlich constant for species *i* at adsorption site B, $Pa^{-\nu_i}$
c_i	molar concentration of species *i* in gas mixture, mol m^{-3}
c_{i0}	molar concentration of species *i* in gas mixture at inlet to adsorber, mol m^{-3}
L	length of packed bed adsorber, m
p_i	partial pressure of species *i* in mixture, Pa
p_t	total system pressure, Pa
q_i	component molar loading of species *i*, mol kg^{-1}
$q_{sat,A}$	saturation loading of site A, mol kg^{-1}
$q_{sat,B}$	saturation loading of site B, mol kg^{-1}
$\bar{q}_i(t)$	*spatially averaged* component molar loading of species *i*, mol kg^{-1}
R	gas constant, 8.314 J mol^{-1} K^{-1}
S_{ads}	adsorption selectivity, dimensionless
t	time, s
T	absolute temperature, K
u	superficial gas velocity in packed bed, m s^{-1}
v	interstitial gas velocity in packed bed, m s^{-1}
z	distance along the adsorber, and along membrane layer, m

Greek letters

ε	voidage of packed bed, dimensionless
ν	exponent in dual-Langmuir-Freundlich isotherm, dimensionless
ρ	framework density, kg m^{-3}
τ	time, dimensionless

Subscripts

i	referring to component *i*

A	referring to site A
B	referring to site B

Table S1. Dual-Langmuir-Freundlich fits for C_2H_4 and C_2H_6 at 296 K in MIL-101-Cr-SO_3Ag.

T-dependent fits for 296 K and 318 K isotherm data

$$b_A = b_{A0}\exp\left(\frac{E_A}{RT}\right); \quad b_B = b_{B0}\exp\left(\frac{E_B}{RT}\right)$$

	Site A				Site B			
	$q_{A,sat}$ mol kg^{-1}	b_{A0} Pa$^{-\nu_i}$	E_A kJ mol^{-1}	ν_A dimensionless	$q_{B,sat}$ mol kg^{-1}	b_{B0} Pa$^{-\nu_i}$	E_B kJ mol^{-1}	ν_B dimensionless
C_2H_4	2.3	6.22×10^{-6}	22	0.35	3.3	4.01×10^{-9}	6	1.46
C_2H_6	8.3	7.06×10^{-8}	13.6	0.84				

Table S2. Langmuir-Freundlich fits for C_2H_4 and C_2H_6 in MIL-101-Cr.

	$q_{A,sat}$ mol kg^{-1}	b_{A0} Pa$^{-\nu_i}$	E_A kJ mol^{-1}	ν_A dimensionless
C_2H_4	5.2	1.83×10^{-11}	35.4	0.95
C_2H_6	7.5	2.47×10^{-7}	10	0.9

Table S3. Langmuir-Freundlich fits for C_2H_4 and C_2H_6 in MIL-101-Cr-SO_3H.

	$q_{A,sat}$ mol kg^{-1}	b_{A0} Pa$^{-\nu_i}$	E_A kJ mol^{-1}	ν_A dimensionless
C_2H_4	6.7	1.31×10^{-6}	7.8	0.82
C_2H_6	6.3	1.2×10^{-7}	13	0.85

The investigation of interaction between ethylene and Ag+ or open metal sites.

Electronic structure calculations were performed to investigate the interaction between ethylene and Ag^+ ion. A $(C_6H_3(CO_2)_2)SO_3Ag$ cluster was considered for this calculation since it is expected that MIL-101-Cr-SO_3Ag contains this moiety. Starting with the sulfonyl terephthalate unit, a silver ion was placed in proximity to the oxygen atoms of the sulfonate group. The Ag^+ ion was optimized to an energetically favorable position within the cluster. The optimization was performed using density functional theory (DFT) with the well-known B3LYP functional. For this calculation, the 6-31G* basis set was used for all C, H, O, and S atoms, whereas the aug-cc-pVDZ-PP basis set[12] was used for Ag since a very large basis set was required to treat the inner electrons of this many-electron species. The optimized position for the Ag^+ ion was discovered to be 2.18 Å from one RSO_3^- oxygen atom and 2.19 Å from another oxygen atom.

Afterwards, an optimized ethylene molecule was placed in proximity to the Ag^+ ion in the $(C_6H_3(CO_2)_2)SO_3Ag$ cluster. The optimization of the C_2H_4–Ag^+ interaction was executed

using DFT using the same functional and basis sets for all atoms as described above. It was observed that the C_2H_4 molecule adsorbed closely to the Ag^+ ion in the cluster. The distances between the Ag^+ ion and the carbon atoms of the C_2H_4 molecule were found to be 2.18 and 2.19 Å. These distances are representative of a strong physisorption interaction. Note, the $C(C_2H_4)$–Ag^+ distances calculated in this work are notably shorter than the distances that were observed for the interaction between a silver ion and the unsaturated carbon atoms of a propylene molecule from previous work.[13]

A similar calculation was performed to examine the interaction between ethylene and an open-metal Cr^{3+} ion. A $[Cr_3O(O_2CH)_6]^+$ cluster, taken from the crystal structure of MIL-101-Cr, was used for this calculation. The SBKJC VDZ ECP[14] basis set was assigned to Cr for the calculations. This is a smaller basis set than what was used for Ag since Cr does not have as many electrons as Ag. A C_2H_4 molecule was placed in the vicinity of one of the Cr^{3+} ions and the molecule was relaxed using the same DFT methods as implemented above. The calculations revealed that the C_2H_4 molecule is further away from the Cr^{3+} ion as compared to the Ag^+ ion. Indeed, the optimized $C(C_2H_4)$–Cr^{3+} distances were observed to be 2.54 and 2.55 Å. This signifies a weaker interaction compared to the aforementioned $C(C_2H_4)$–Ag^+ distances. All calculations were performed using the NWChem software.[15]

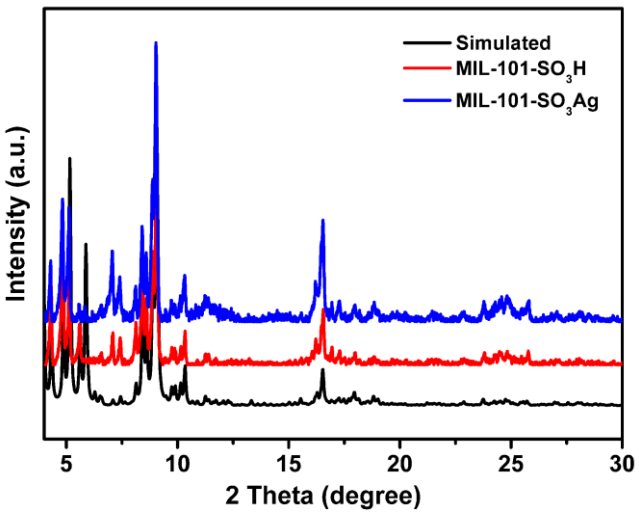

Fig. S1. Comparison of XRD of simulated MIL-101-Cr-SO_3H (black), MIL-101-Cr-SO_3H (red), and MIL-101-Cr-SO_3Ag (blue).

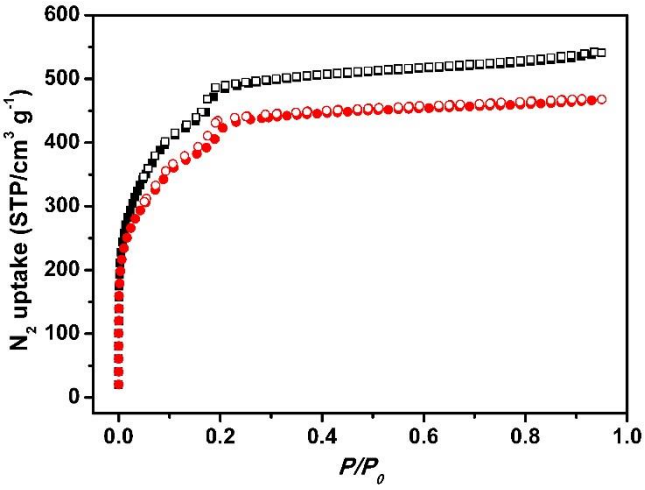

Fig. S2. Comparison of N_2 sorption MIL-101-Cr-SO_3H (black), MIL-101-Cr-SO_3Ag (red).

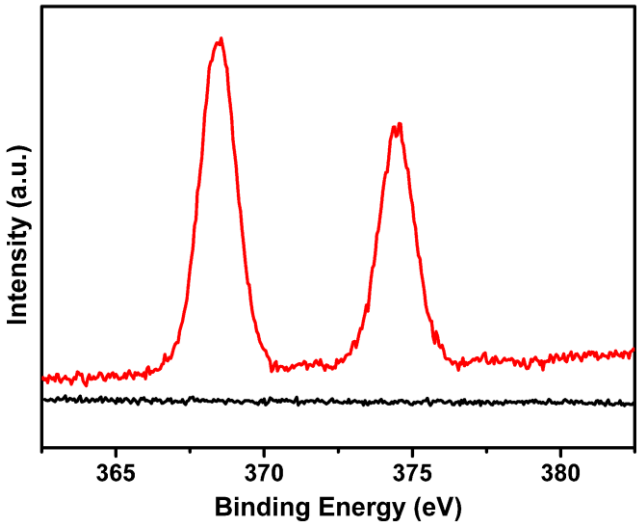

Fig. S3. Comparison of Ag(I) XPS of MIL-101-Cr-SO_3H (black) and MIL-101-Cr-SO_3Ag (red).

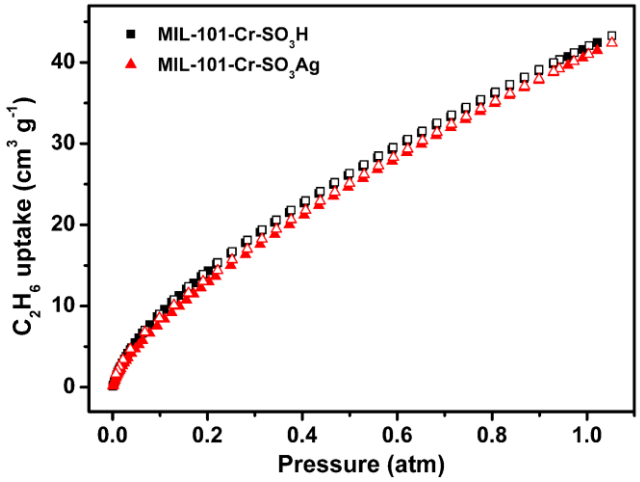

Fig. S4. Comparison of ethane sorption isotherms of MIL-101-Cr-SO_3H (black), and MIL-101-Cr-SO_3Ag (red) at 296 K.

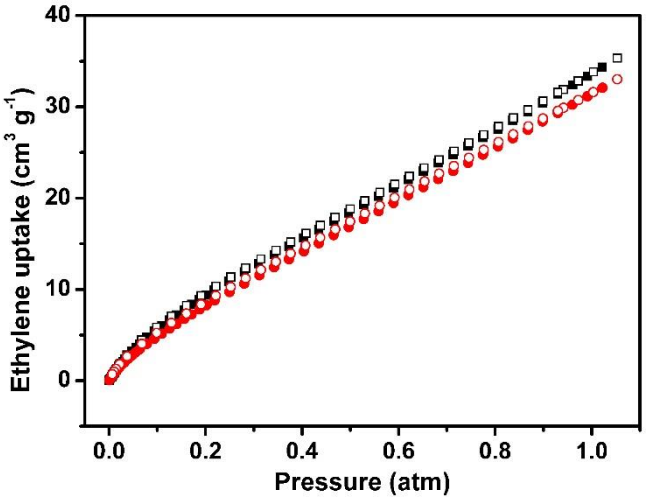

Fig. S5. Comparison of ethane sorption isotherms of MIL-101-Cr-SO_3H (black), and MIL-101-Cr-SO_3Ag (red) at 318 K.

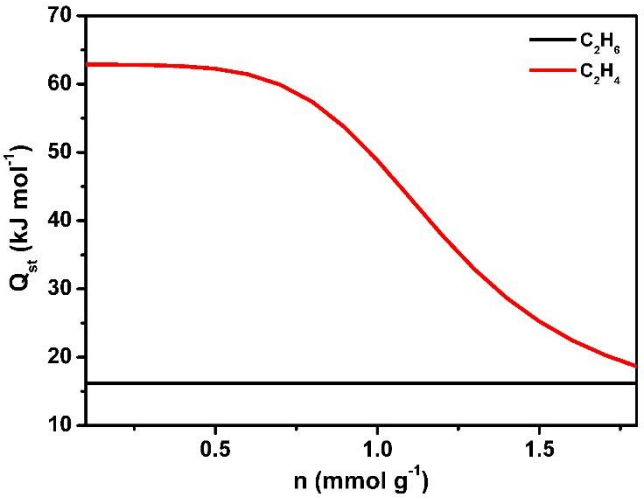

Fig. S6. Comparison of isosteric heats of adsorption for ethylene (red) and ethane (black) in MIL-101-Cr-SO_3Ag.

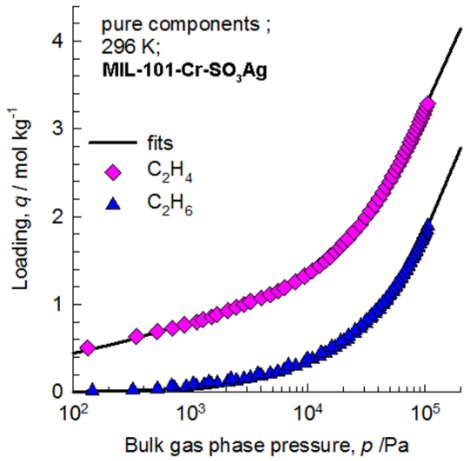

Fig. S7. Comparison of the experimentally determined component loadings for C_2H_4, and C_2H_6 on MIL-101-Cr-SO_3Ag at 296 K with the isotherm fits using parameters specified in Table S1.

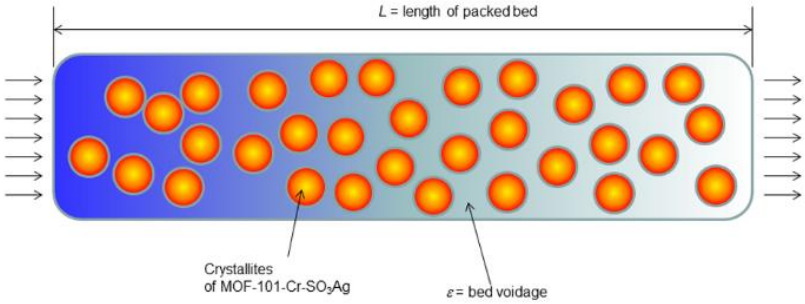

Fig. S8. Schematic of a packed bed adsorber. The parameter values used in the simulations presented here are: L = 0.12 m; voidage of bed, ε = 0.75; interstitital gas velocity, v= 0.003 m/s, superficial gas velocity, u = 0.00225 m/s.

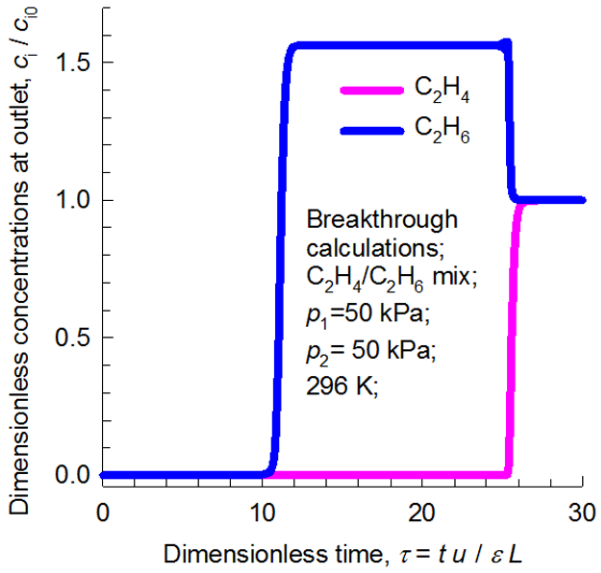

Fig. S9. Transient breakthrough of an equimolar C_2H_4/C_2H_6 mixture in an adsorber bed packed with MIL-101-Cr-SO_3Ag in the adsorption phase of a PSA operation. The inlet gas is maintained at partial pressures $p_1 = p_2 = 50$ kPa, at a temperature of 296 K.

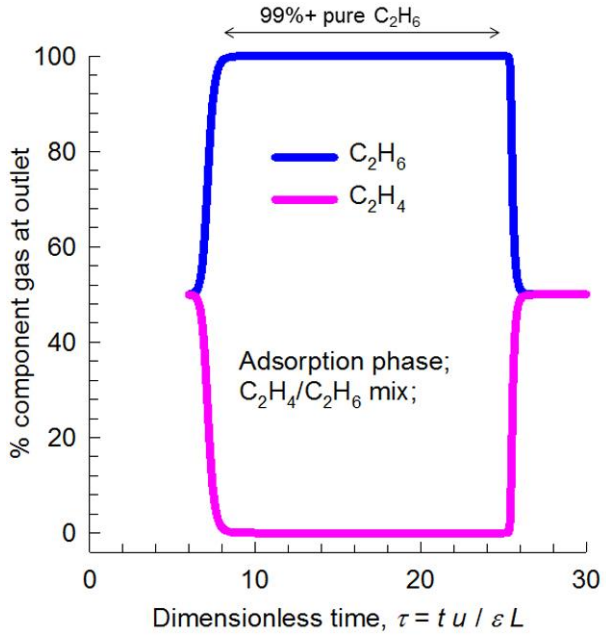

Fig. S10. % C_2H_6 in the outlet gas of an adsorber bed packed with MIL-101-Cr-SO_3Ag in the adsorption cycle. The inlet gas is maintained at partial pressures $p_1 = p_2 = 50$ kPa, at a temperature of 296 K.

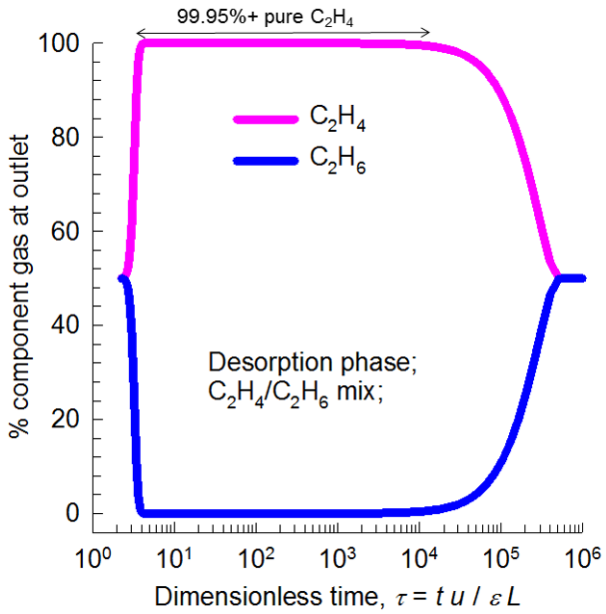

Fig. S11. % C_2H_4 in the outlet gas of an adsorber bed packed with MIL-101-Cr-SO_3Ag in the desorption cycle. The contents of the bed, that is equilibrated at partial pressures $p_1 = p_2 = 50$ kPa, at a temperature of 296 K is purged by inert gas. For the calculations presented in the graph, the inert gas is not included in the calculation of the % compositions.

Reference.

(1) G. Akiyama, R. Matsuda, H. Sato, M. Takata, and S. Kitagawa, *Adv. Mater.*, 2011, **23**, 3294.

(2) A. L. Myers, J. M. Prausnitz, *A.I.Ch.E.J.*, 1965, **11**, 121.

(3) D. M. Ruthven, Principles of Adsorption and Adsorption Processes, John Wiley: New York, 1984.

(4) D. M. Ruthven, S. Farooq, K. S. Knaebel, Pressure swing adsorption, VCH Publishers: New York, 1994.

(5) R. T. Yang, Gas separation by adsorption processes, Butterworth: Boston, 1987.

(6) D. D. Do, Adsorption analysis: Equilibria and kinetics, Imperial College Press: London, 1998.

(7) L. J. P. van den Broeke, R. Krishna, *Chem. Eng. Sci.*, 1995, **50**, 2507.

(8) K. S. Walton, M. D. LeVan, *Ind. Eng. Chem. Res.*, 2003, **42**, 6938.

(9) R. Krishna, R. Baur, *Sep. Purif. Technol.*, 2003, **33**, 213.

(10) R. Krishna, *Microporous Mesoporous Mater.*, 2014, **185**, 30.

(11) R. Krishna, J. R. Long, *J. Phys. Chem. C*, 2011, **115**, 12941.

(12) K. A. Peterson, C. Puzzarini, *Theor. Chem. Acc.*, 2005, **114**, 283.

(13) K. C. Kim, C. Y. Lee, D. Fairen-Jimenez, S. T. Nguyen, J. T. Hupp, R. Q. Snurr, *J. Phys. Chem. C*, 2014, **118**, 9086.

(14) (a) W. J. Stevens, M. Krauss, H. Basch, P. G. Jasien, *Can. J. Chem.*, 1992, **70**, 612; (b) T. R. Cundari, W. J. Stevens, *J. Chem. Phys.*, 1993, **98**, 5555.

(15) M. Valiev, E. Bylaska, N. Govind, K. Kowalski, T. Straatsma, H. V. Dam, D. Wang, J. Nieplocha, E. Apra, T. Windus, W. de Jong, *Comput. Phys. Commun.*, 2010, **181**, 1477.